Ab Initio Molecular Dynamical Investigation of the Finite Temperature Behavior of the Tetrahedral Au_{19} and Au_{20} Clusters

Sailaja Krishnamurty, Ghazal S. Shafai, and D. G. Kanhere*

Department of Physics and Centre for Modeling and Simulation, University of Pune, Ganeshkhind, Pune 411 007, India

B. Soulé de Bas and M. J. Ford

Institute for Nanoscale Technology, University of Technology, Sydney P.O. Box 123, Broadway, NSW 2007, Australia

Received: July 26, 2007

Density functional molecular dynamics simulations have been carried out to understand the finite temperature behavior of Au_{19} and Au_{20} clusters. Au_{20} has been reported to be a unique molecule having tetrahedral geometry, a large HOMO−LUMO energy gap, and an atomic packing similar to that of the bulk gold (Li, J.; et al. *Science* **2003**, *299*, 864). Our results show that the geometry of Au_{19} is exactly identical with that of Au_{20} with one missing corner atom (called a vacancy). Surprisingly, our calculated heat capacities for this nearly identical pair of gold clusters exhibit dramatic differences. Au_{20} undergoes a clear and distinct solid-like to liquid-like transition with a sharp peak in the heat capacity curve around 770 K. On the other hand, Au_{19} has a broad and flat heat capacity curve with continuous melting transition. This continuous melting transition turns out to be a consequence of a process involving a series of atomic rearrangements along the surface to fill in the missing corner atom. This results in a restricted diffusive motion of atoms along the surface of Au_{19} between 650 to 900 K during which the shape of the ground state geometry is retained. In contrast, the tetrahedral structure of Au_{20} is destroyed around 800 K, and the cluster is clearly in a liquid-like state above 1000 K. Thus, this work clearly demonstrates that (i) the gold clusters exhibit size sensitive variations in the heat capacity curves and (ii) the broad and continuous melting transition in a cluster, a feature that has so far been attributed to the disorder or absence of symmetry in the system, can also be a consequence of a defect (absence of a cap atom) in the structure.

I. Introduction

Recently discovered clusters and nanostructures of gold are found to have a rich chemistry with potential applications in materials science,[1] medicine,[2] and the area of catalysis.[3,4] In particular, small clusters of gold have attracted interest as tips and contacts in molecular electronic circuits[5] and also as chemical catalysts.[6] Experimentally, even a small cluster such as Au_8 has been reported to catalyze the oxidation reaction of CO.[7] However, these properties are reported to have strong size-sensitive variations. Another factor influencing the application of gold clusters is their thermal stability. It is noted that several Au clusters undergo structural transformation or tend to grow readily by migrating and merging[8] under high-temperature conditions (500 K and above). These effects have important consequences in the applications involving elevated temperatures and the growth mechanisms of clusters. In this context, a study on the finite temperature behavior of Au clusters is of considerable importance.

Since the pioneering reports on the possible applications of gold clusters, a large amount of experimental[9] and theoretical work[10] has been devoted to understand the structural and electronic properties of Au_n ($n \leq 50$) clusters. These reports have demonstrated that gold clusters have very different physical and chemical properties as compared to their bulk counterpart. A more recent exciting report has shown photoelectron spectroscopic evidence of hollow golden cages with an average diameter of 5.5 Å in the size range of 16 to 18 atoms.[11] These predictions were further supported by the theoretical calculations in the same report. However, Au_{20} is the most intriguing gold cluster reported so far.[12] Experimental studies[11−13] report this cluster to have a pyramidal structure (tetrahedral symmetry) with each of the four faces representing the (111) surface of the Face Centered Cubic (FCC) gold. It is reported to have a large energy gap between the Highest Occupied Molecular Orbital (HOMO) and Lowest Occupied Molecular Orbital (LUMO). This energy gap is greater than that of C_{60} suggesting it to be highly stable and chemically inert. On the other hand, its structure with high surface area and large fraction of corner sites with low atomic coordination is expected to provide ideal surface sites to bind various molecules such as CO, O_2, and CO_2 for catalysis. The structure of Au_{19} is also seen to be very similar to that of Au_{20} with one missing corner atom. In this context, it is interesting to have an understanding on the thermal stability of these two gold clusters having an atomic packing similar to that of bulk gold. Hence, in the present work, we study the finite temperature behavior of Au_{19} and Au_{20} using the first principles Molecular Dynamics (MD) simulations.

While several experimental and theoretical studies have been devoted to understand the ground state geometries and chemical reactivity of gold clusters, there are very few reports on the

* Address correspondence to this author.

10.1021/jp075896+ CCC: $37.00
Published on Web 10/03/2007

finite temperature properties of gold clusters.[14,15] The classical MD simulations by Landman and co-workers[14,15] on medium-sized Au clusters (150−1500 atoms) indicated that the clusters in this size range undergo a solid-to-solid structural transformation around 700 K, before eventually melting around 780 K. This is at a much lower value as compared to the bulk melting temperature of 1377 K. However, to the best of our knowledge, only one ab initio molecular dynamics study[16] attempting to understand the finite temperature behavior of Au clusters has been reported so far.

As the cluster size reduces, the electronic effects play a more explicit role in controlling the structural and thermal properties of the clusters. This is amply demonstrated by several first principles molecular dynamics simulations,[17−25] which have successfully explained various experimental findings[26−34] on the finite temperature behavior of sodium, tin, gallium, and aluminum clusters. These experimental studies have brought out various interesting phenomena such as higher than bulk melting temperatures in Ga and Sn clusters,[30,31] and strong size dependent variations in the melting temperatures of Ga and Al clusters.[32,33] However, the most surprising experimental finding is the size-sensitive behavior of the shape of the heat capacities where addition of even one atom is seen to result in a dramatic change of shape, prompting some of the clusters to be called "Magic Melters".[32] This means that while some clusters do undergo a conventional and clear melting transition, others undergo a near-continuous transition making it very difficult to identify any meaningful transition temperature. In a recent communication,[18] we have clearly demonstrated that a cluster with local "order" (an island of atoms connected with equal bond strengths) displays a well-characterized melting transition with a distinct peak in the heat capacity curve, while a "disordered" cluster is seen to undergo a continuous transition with a flat heat capacity curve. Further, it is noted that this size-sensitive nature in small clusters is related to the evolutionary pattern seen in their ground states and is seen to exist in clusters of sodium, gallium, and aluminum.[25,35,36]

In what follows, we show that this dramatic variation in the shape of the heat capacity curve is also observed in the present pair of gold clusters, viz., Au_{19} and Au_{20}. This observation has also thrown light on additional factors responsible for a continuous melting transition in clusters. As we shall see, in contrast to gallium or aluminum clusters, the flat or broad heat capacity curve in Au_{19} is attributed to a "vacancy" in the surface (or a surface defect). This "vacancy" results in a chain of atomic rearrangements leading to a restricted diffusion of atoms along the surface. In contrast, Au_{20} undergoes a relatively sharp melting transition with a clear peak in the heat capacity curve around 770 K. Thus, these results bring out an understanding not only of additional factors contributing to the broad melting transition in clusters but also of the relative thermal stability of these unique tetrahedral gold clusters.

It may be noted that the present work is based on the Density Functional Theory (DFT) method. We also use plane wave basis whose advantages for carrying out accurate MD simulations are well established.[37] Indeed, an excellent agreement has been obtained for properties such as melting temperature, latent heat, and the shapes of the specific heat capacity curves for clusters of sodium (delocalized charge density),[24] gallium and tin (covalently bonded systems),[21,35] and aluminum.[36] It may be further noted that the ground state geometries found here and for Au_n ($n = 16-21$) by DFT calculations agree with the experimentally observed geometries.[11−13] Thus, the accuracy of the DFT method on Au clusters in this size range is well tested by now.

II. Computational Details

We have optimized about 300 geometries for each of the clusters, to obtain the ground state geometry and several low-energy isomers. The initial configurations for the optimization were obtained by carrying out a constant-temperature dynamics of 100 ps each at various temperatures between 400 and 1600 K. Once the ground state geometry is obtained, thermodynamic simulations are performed by using Born−Oppenheimer MD based on the Kohn−Sham formulation of Density Functional Theory (DFT).[38] The ionic phase space of the clusters is sampled classically in a canonical ensemble according to the method proposed by Nóse.[39] The mass of the Nóse thermostat is chosen such that the characteristic frequency of the thermostat falls within the range of the vibrational eigen frequencies of the system. The potential energy distribution obtained by the Nóse thermostat with this mass is further seen to be statistically similar to the one generated by using an isokinetic velocity scaling algorithm.[40] The MD simulations have been carried out by using Vanderbilt's ultra-soft pseudopotentials[41] within the Local Density Approximation (LDA) for describing the core−valance interactions as implemented in the vasp package.[42] Our choice of functional was based on the fact that the energetics of the gas-phase Au clusters using LDA-DFT calculations[10] was seen to match more closely with that of the CCSD(T) calculations.[43] An energy cutoff of 13.21 Ry is used for the plane wave expansion of Au. We have used cubic super cells of length 20 Å and have ensured that the results converge with respect to a further increase in the energy cutoff and size of the simulation box.

Following the finite temperature study, the ionic heat capacity of both clusters is computed by using the multiple histogram (MH) method.[44,45] The computation of the heat capacity with the MH technique is sensitive to the number of temperatures at which the thermodynamic behavior of the cluster is simulated. The range and the number of temperatures must be chosen so as to have an adequate overlap of potential energy distribution. To have a reliable sampling, we split the total temperature range from 400 to 1600 K into at least 15 different temperatures for both clusters. We maintain the cluster at each temperature for a period of at least 100 ps after equilibration, leading to a total simulation time of around 1.3 ns. We have further ensured that our heat capacity curve does not change with the addition of additional temperatures between 400 and 1600 K. The MH method and the various errors associated with it are discussed in detail in one of the earlier works.[21]

An important source of error in MD simulations is the limited statistics for calculating the finite temperature properties. It may be noted that the ab initio nature of the method puts a restriction on the simulation time scales. An examination of the convergence of various thermodynamic indicators has indicated that a simulation time of 70 ps is sufficient enough in the present case. During the MD simulations, the small amount of angular momentum of the clusters is removed from the equation of the ionic motion at every step. Another way to remove the angular momentum from the clusters is described in one of the recent works.[46]

Various other thermodynamic indicators such as the mean-squared displacements (MSDs) of ions and the root-mean-squared bond-length fluctuation (RMS-BLF or δ_{rms}) are also computed. For the sake of completeness we briefly discuss these

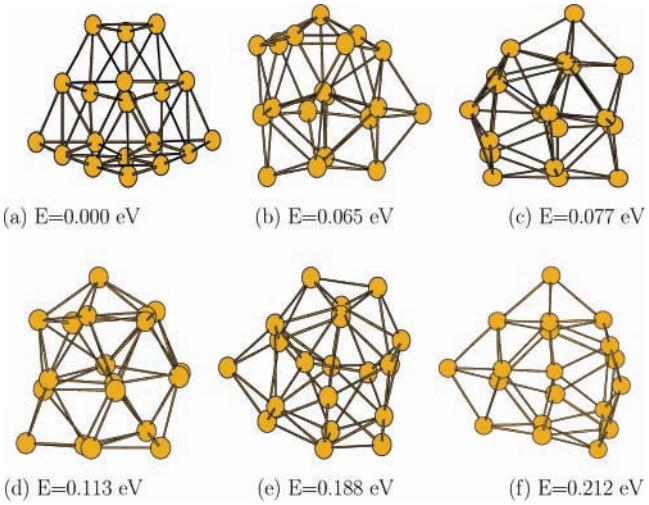

Figure 1. The ground state geometry and low-lying isomers of Au_{19}. The energy below is the difference in total energy of the isomer with respect to the ground state energy.

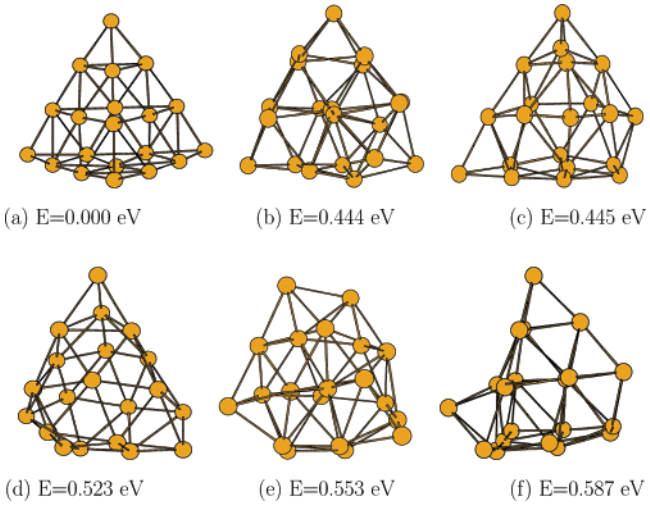

Figure 2. The ground state geometry and low-lying isomers of Au_{20}. The energy below is the difference in total energy of the isomer with respect to the ground state energy.

parameters. The parameter δ_{rms} is a measure of the fluctuations in the bond lengths averaged over all the atoms and over the total time span. It is defined as

$$\delta_{rms} = \frac{2}{N(N-1)} \sum_{i>j} \frac{(\langle r_{ij}^{\,2}\rangle_t - \langle r_{ij}\rangle_t^{\,2})^{1/2}}{\langle r_{ij}\rangle_t} \qquad (1)$$

where N is the number of atoms in the system, r_{ij} is the distance between atoms i and j, and $\langle ... \rangle_t$ denotes a time average over the entire trajectory. The MSD is another widely used parameter for analyzing a solid-like-to-liquid-like transition. In the present work, we calculate the mean-squared displacements for individual atoms, which is defined as

$$\langle \mathbf{r}_I^{\,2}(t)\rangle = \frac{1}{M} \sum_{m=1}^{M} [\mathbf{R}_I(t_{0m}+t) - \mathbf{R}_I(t_{0m})]^2 \qquad (2)$$

where $\mathbf{R}_I$ is the position of the Ith atom and we average over M different time origins t_{0m} spanning the entire trajectory. The MSD indicates the displacement of an atom in the cluster as a function of time. In the solid-like region, all atoms perform oscillatory motion about fixed points resulting in negligible MSDs of individual atoms from their equilibrium positions. In a liquid-like state, on the other hand, atoms diffuse throughout the cluster and the MSDs eventually reach a saturated value of the order of the square of the cluster radius. More technical details concerning the extraction of thermodynamic averages, indicators, and computation of the heat capacity curve can be found in previous work.[45]

III. Results and Discussion

We begin with a discussion on the ground state geometries and some representative low-lying isomers of Au_{19} and Au_{20} which are shown in the Figures 1 and 2, respectively. It is clearly seen from these figures that the ground state geometry of Au_{20} (Figure 2a) is a tetrahedron. The ground state geometry of Au_{19} (Figure 1a) differs from that of Au_{20} by a single missing vertex atom of the tetrahedron. This is in agreement with the recent experimental and theoretical predictions.[11] Quite clearly both structures are symmetric, with ordered triangles stacked over one another. The rest of the geometric parameters such as bond lengths, bond angles, and dihedral angles are almost identical

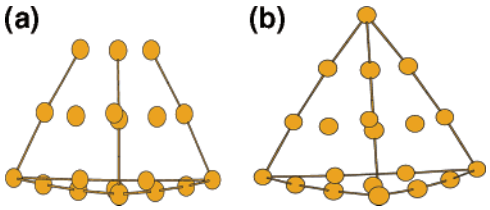

Figure 3. The distribution of shortest bonds (2.63 Å) in Au_{19} and Au_{20}. The rest of the interatomic bond distances (for the first nearest nearest neighbor) in both the clusters are 2.75 Å.

in both ground state geometries. Thus, Au_{19} can be considered as Au_{20} with a vertex defect.

The atoms in Au_{19} as well as Au_{20} are bonded to their first nearest neighbors with bond distances of either 2.63 Å (shortest bonds in the cluster) or 2.75 Å (next shortest bonds). It is interesting to display the connectivity of the shortest bonds to bring out the differences in them. Parts a and b of Figure 3 show the distribution of shortest bonds (2.63 Å) for the case of Au_{19} and Au_{20}, respectively. Clearly, the shortest bonds are distributed only along the surface of both clusters and form a closed network in Au_{20}, while in Au_{19} they form an open network due to the missing atom. It turns out that the presence of the vertex defect and open skeleton of shortest bonds in Au_{19} play a significant role in the finite temperature behavior of the cluster around 650 K and initiate a set of restricted atomic rearrangements on the surface.

The low-lying isomers of Au_{19} (shown in Figure 1b−f) are clearly devoid of a regular triangular arrangement of atoms seen in the ground state configuration. The first low-lying isomer of Au_{19} (Figure 1b) is nearly 0.065 eV higher in energy as compared to the ground state configuration. Au_{19} has several isomers with continuous energy distribution between 0.065 and 0.7 eV, some of which are shown in Figure 1, parts c−f. This can be contrasted with first low-lying isomer of Au_{20} (shown in Figure 2b), which is almost 0.44 eV higher than the ground state geometry. This structure has one central atom and the rest of the 19 atoms arrange around this central atom so as to have a highly deformed tetrahedron. This configuration is degenerate with the hollow cage configuration of Au $_{20}$ (Figure 2c). The fact that there are a couple of isomers well separated from the ground state geometry correlates very well with the existence of a relatively sharp and well-defined peak in the heat capacity curve of Au_{20}. Bixon and Jortner[47] have established an explicit

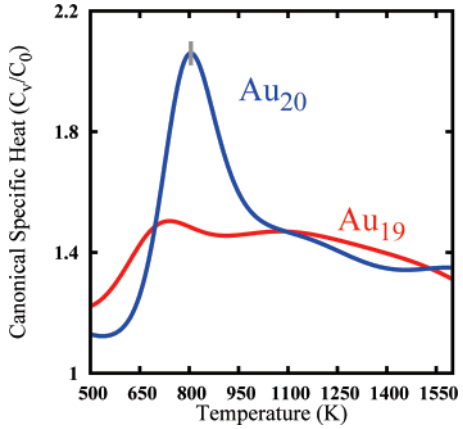

Figure 4. The heat-capacity curves of Au_{19} and Au_{20}. $C_0 = (3N - 9/2)K_B$ is the zero-temperature classical limit of the rotational plus vibrational canonical specific heat. The bar at the peak of the Au_{20} curve indicates the maximum estimated error in the height. The peak positions are stable to within ±50 K.

analytical relationship between melting characteristics and the internal energies of the isomers. They show that clusters having a large energy gap within the isomer distribution and a considerable spread of the high-lying isomers (which is the case for Au_{20}) exhibit a clear transition in their caloric curve, while clusters having a continuous distribution of isomers do not exhibit such a clear melting transition. Our calculations are consistent with their observations. It also may be noted that similar features in the heat capacity curves were also observed in the case of a few other clusters by using Lennard-Jones potentials.[48] Some other representative low-lying isomers of Au_{20} are shown in Figure 2d−f. We also note that the atoms in all the high-energy configurations of both clusters are bonded to each other through a much wider and continuous range of Au−Au bond lengths (ranging between 2.67 and 2.90 Å) as compared to those in the ground state geometry.

Now, we present the finite temperature behavior of both clusters. We begin with a discussion on the calculated heat capacity curves which is shown in Figure 4. The figure brings out a remarkable feature, viz., a significant size-sensitivity nature of the heat capacity curves. The heat capacity curve of Au_{20} has a clear and recognizable peak around 770 K, with a width of about 250 K. In contrast, the heat-capacity curve of Au_{19}, a cluster with a vacancy, shows a broad and almost continuous solid-to-liquid transition between 650 and 1200 K. Thus, this is yet another example of dramatic change in the shape of the heat capacity curve with the addition of a single atom. As already noted this size-sensitive nature has been observed earlier in Ga, Al clusters experimentally.[32,33]

It is possible to make a detailed analysis of the ionic motion by examining the trajectories of the clusters. An analysis of the ionic motions of Au_{19} reveals the cluster to vibrate around its ground state geometry until 600 K. Around 650 K, the cluster undergoes a peculiar structural rearrangement so as to fill in the vacancy (the apex atom). The snapshots of this structural rearrangement are shown from Figure 5a to Figure 5e. Figure 5a shows Au_{19} with a missing cap atom. Note that, at the end of the structural rearrangement (Figure 5e), the vacancy that is present on the top in Figure 5a is shifted to the bottom edge. We denote the edge consisting of atoms "A", "B", and "C" as the reference edge. Coming to the details of the structural rearrangement, as the cluster evolves around 650 K, it is seen that these atoms in the reference edge push themselves upward (see Figure 5b to Figure 5d). The rest of atoms in the cluster undergo minor displacements around their equilibrium positions

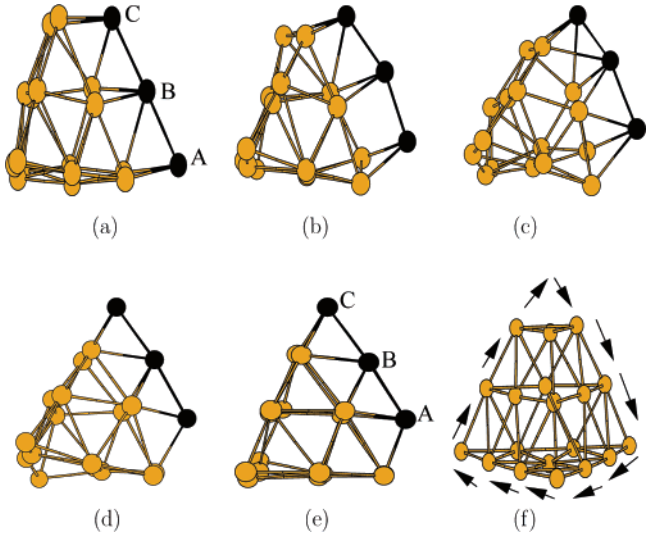

Figure 5. (a−e) Snapshots of restricted rearrangement of atoms in Au_{19} around 650 K. (f) Arrows depict the continuous atomic rearrangements that take place to fill in the missing cap atom between 700 and 900 K.

during this process. At the end of this rearrangement (see Figure 5e), it is seen that the top edge atom (atom "C") in Au_{19} moves to cap the missing vertex atom seen in Figure 5a. The next edge atom ("B") moves up to occupy the position initially occupied by atom "C" and atom "A" occupies the position occupied by "B". Now this creates a vacancy or defect at the position initially occupied by the atom "A". Thus, we now have a Au_{19} cluster that is rotated by 90° in the anticlockwise direction (Figure 5e) with respect to Figure 5a.

Around 650 K, only a single edge is displaced so as to cap the missing vertex atom. Between 700 and 900 K, we see a continuous displacement of atoms along all the edges as shown in Figure 5f as the vacancy is shifted from one vertex to the other vertex. A remarkable feature of this motion is that the overall shape of the cluster remains approximately tetrahedron with a missing cap. Around 1000 K, the tetrahedron structure is destroyed and the cluster visits its first and second high-energy configurations. The cluster finally melts completely above 1200 K. This leads to a broad feature (between 650 and 1200 K) in its heat capacity curve.

In contrast, the ionic motion of Au_{20} shows all the atoms to vibrate around their initial positions until about 750 K. The cluster undergoes a structural transformation from the ground state geometry to the first isomer shown in Figure 2b around 800 K. The cluster visits other isomers around 900 K and melts completely above 1000 K leading to a clear and relatively narrow melting transition.

This contrasting behavior is brought out more clearly by examining the MSDs of the individual atoms. It may be recalled that we have ensured that our clusters do not rotate and hence the MSD values that we report correspond to the absolute displacement of the ion from its original position. In Figure 6, we show the MSDs of individual atoms in both clusters in the temperature range of 450−1000 K. It is clear from parts a and b of Figure 6 that atoms in both clusters vibrate around their equilibrium positions at 450 K. Around 650 K, the rearrangement of atoms along one edge in Au_{19} is reflected in slightly higher mean-squared displacements (around 3 Å) in Figure 6c. These values increase continuously in Au_{19} as shown by the typical behavior around 800 K. In contrast, the MSD values in Au_{20} are negligible until 750 K ($<$0.5 Å) and the values increase sharply around 800 K. It is precisely at this temperature that

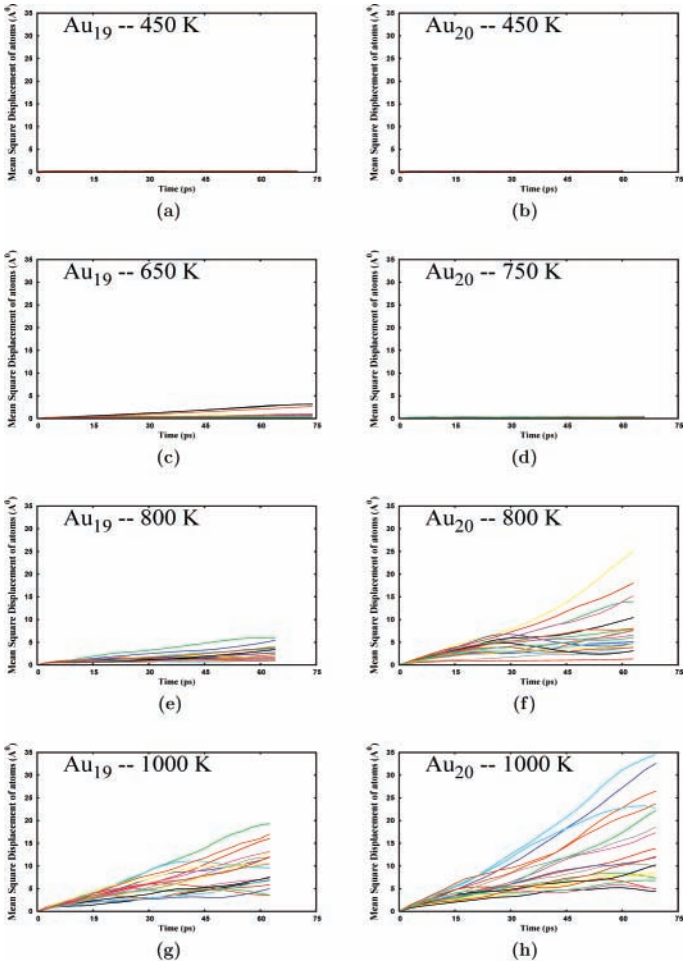

Figure 6. The root-mean-squared displacements of atoms with respect to the simulation time (ps) in Au_{19} at various temperatures.

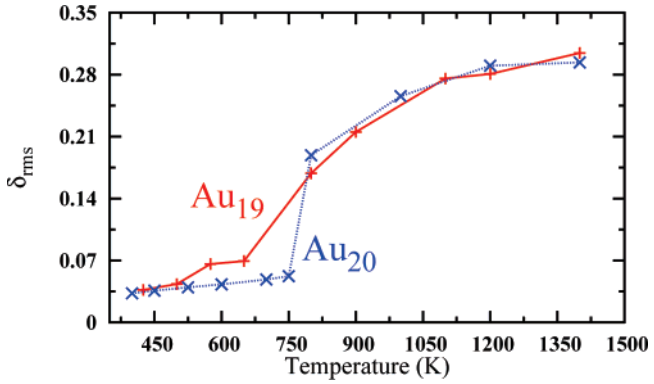

Figure 7. δ_{rms} of Au_{19} and Au_{20}.

the tetrahedron is destroyed. The MSDs of Au_{19} and Au_{20} saturate around 35 Å at 1200 and 1000 K, respectively, indicating the presence of a liquid-like state.

This contrasting behavior is somewhat weakly reflected in the average root-mean-squared bond-length fluctuation (δ_{rms}) of Au_{19} and Au_{20}, which is in any case a quantity averaged out over all the atoms. In Figure 7 we show the δ_{rms} for both the clusters. As expected Au_{20} shows a sharp transition indicated by a jump in the δ_{rms} value from 0.07 to 0.20.

As already mentioned in Section II (Computational Details), all of the above calculations were carried out at a local density approximation. However, to assess the role of exchange correlation functional, we have obtained around 30 isomers for each of the clusters with Generalized Gradient Approximation (GGA) using the Perdew−Burke−Ernzerhof functional. All the clusters were optimized by using the Projector Augumented Wave (PAW) psuedopotential. An analysis of these optimized configurations reveals that the ground state geometries of Au_{19} and Au_{20} remain unaffected by the change of the exchange correlation functional. There are small variations in the bond lengths, with GGA predicting slightly longer bond distances (∼3%) as compared to those by LDA. The rest of the structural features such as distribution of the shortest bonds remain the same.[49] An isomer analysis reveals that the first low-lying isomers of Au_{19} and Au_{20} are identical with those obtained by LDA. The first low-lying isomer of Au_{19} (Figure 1b) is about 0.081 eV higher in energy with respect to the ground state geometry (see Figure 1a), while in the case of Au_{20} the first low-lying isomer is about 0.54 eV higher in energy. Thus, there is a shift in the relative energies of first low-lying isomers with respect to the ground state geometry as compared to LDA. The first high-energy isomer is followed by a "continuous distribution" of isomers in both clusters as is the case in LDA.

To assess the effect of the GGA functional on the finite temperature properties, we have carried out representative simulations on these clusters at four different temperatures between 600 and 1000 K. This region corresponds to the predicted solid-to-liquid transition by the LDA method. These simulations were performed for a time period of 40 ps. From the finite temperature calculations using GGA, we have computed the multiple histograms (MH), which is a crucial input for the calculation of the heat capacity curve. The MH is obtained when the potential energy at these temperatures is sampled according to a canonical distribution. The multiple histograms obtained from the GGA simulations were found to

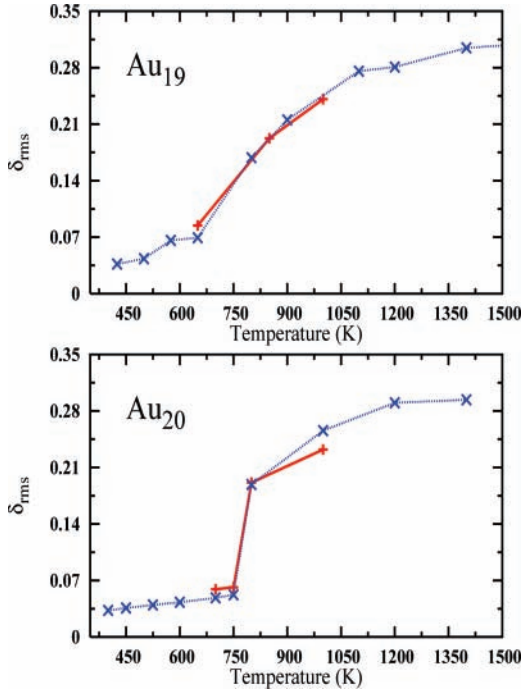

Figure 8. δ_{rms} of Au_{19} and Au_{20} calculated from GGA and LDA simulations. The dotted line is the δ_{rms} calculated from LDA while the solid line is the δ_{rms} calculated from GGA.

be statistically identical with the ones obtained from the LDA calculation (figure not shown). In addition to the multiple histograms, we have also calculated δ_{rms}, which is one of the traditional thermodynamic indicators. In Figure 8, we present the δ_{rms} (Lindemann criterion) calculated from GGA and LDA at four different temperatures. The figure clearly shows that δ_{rms} obtained from both approximations is nearly the same. Finally, an analysis of the ionic motion of Au_{19} between 650 and 900 K at the GGA level reveals an identical restricted diffusive motion of the atoms along the edge to fill in the missing vacancy (see Figure 5). Thus, the melting properties (melting temperatures as well as melting characteristics) of both clusters remain unaffected by the type of exchange correlation functional used.

IV. Summary and Conclusions

In this work, we have presented the results of first principle molecular dynamics simulations on Au_{19} and Au_{20}, clusters which have atomic packing similar to that of bulk gold. In spite of the fact that the geometry of both clusters is nearly identical except for a single vertex atom, they exhibit dramatic differences in the shape of their heat capacity curves. We have shown that these differences are induced by vacancy. The vacancy in Au_{19} induces a restricted diffusive motion along the surface of the cluster leading to a continuous melting transition. In contrast, Au_{20} exhibits a sudden and clear melting transition. These melting properties were found to be unaffected by the type of exchange correlation functional. It may be noted that such a size-sensitive nature of the heat capacity curves has been observed experimentally in Al and Ga clusters and in Na clusters during the ab initio molecular dynamic simulations. In these studies the size-sensitive nature of the heat capacity curves was attributed to the nature of the "disorder" in the ground state geometry. The present work clearly shows that this size-sensitive behavior is also driven by the vacancy in the otherwise perfect and symmetric "lattice". The work also demonstrates the size-sensitive variations in the melting characteristics to be generic in nature. Finally, the contrasting finite temperature behavior reported in the present gold clusters could have several implications in the applications of these clusters and is a topic of further research interest.

Acknowledgment. G.S. and D.G.K. thank the Indo French Center For Promotion of Advanced Research (IFCPAR−CEFIPRA) for partial financial support (Project No. 3104-2). The authors thank Kavita Joshi for useful discussions. M.J.F. thanks the Australian Research Council (ARC) for financial support, the Australian Centre for Advanced Computing and Communications(AC3), and the Australian Partnership for Advanced Computing (APAC) for computing facilities. B.S. thanks the ARC for an International Postgraduate Research Scholarship (IPRS).

References and Notes

(1) Dyson, P. J.; Mingos, D. M. P. *Gold. Progress in Chemistry, Biochemistry and Technology*; Schmidbaur, H., Ed.; Wiley, New York, 1999; p 511.
(2) Shaw, C. F., III *Chem. Rev.* **1999**, *99*, 2589.
(3) Teles, J. H.; Brode, S.; Chabanas, M. *Angew. Chem.* **1998**, *99*, 2589.
(4) Hashmi, A. S. K. *Gold Bull.* **2003**, *36*, 3.
(5) Fan, F.-R. F.; Bard, A. J. *Science* **1997**, *277*, 1791.
(6) Valden, M.; Lai, X.; Landman, D. W. *Science* **1998**, *281*, 1647.
(7) Pyykko, P. *Angew. Chem., Int. Ed.* **2004**, *43*, 4412.
(8) Sutter, E.; Sutter, P.; Zhu, Y. *Nano Lett.* **2005**, *5*, 2092.
(9) Gilb, S.; Weis, P.; Furche, F.; Ahlrichs, R.; Kappes, M. M. *J. Chem. Phys.* **2002**, *116*, 4094.
(10) Gilb, S.; Weis, P.; Furche, F.; Ahlrichs, R.; Kappes, M. M. *J. Chem. Phys.* **2002**, *116*, 4094. Walker, A. V. *J. Chem. Phys.* **2005**, *122*, 094310. Zhao, J.; Yang, J.; Hou, J. G. *Phys. Rev. B* **2003**, *67*, 085404. Olson, R. M.; Varganov, S.; Gordon, M. S.; Metiu, H.; Chretien, S.; Piecuch, P.; Kowalski, K.; Kucharski, S. A.; Musial, M. *J. Am. Chem. Soc.* **2005**, *127*, 1049. de Bas, B. S.; Ford, M. J.; Cortie, M. B. *J. Mol. Struct.* **2004**, *686*, 193. Mills, G.; Gordon, M. S.; Metiu, H. *J. Chem. Phys.* **2003**, *118*, 4198. Häkkinen, H.; Landman, U. *Phsy. Rev. B* **2000**, *62*, 2287. Häkkinen, H.; Yoon, B.; Landman, U.; Li, X.; Zhai, H.-J.; Wang, L.-S. *J. Phys. Chem. A* **2003**, *107*, 6168. Remacle, F.; Kryachko, E. S. *J. Chem. Phys.* **2005**, *122*, 044304. Ford, M. J.; Hoft, R. C.; McDonagh, A. *J. Chem. Phys.* **2005**, *109*, 20387. de Bas, B. S.; Ford, M. J.; Cortie, M. B. *THEOCHEM* **2004**, *193*, 686; Wang, J.; Jellinek, J.; Zhao, J.; Chen, Z.; King, B.; von Rague Schleyer, P. *J. Phys. Chem. A* **2005**, *109*, 9265. Yoon, B.; Koskinen, P.; Huber, B.; Kostko, O.; von Issendroff, B.; Hakkinen, H.; Moseler, M.; Landman, U. *Chem. Phys. Chem.* **2007**, *8*, 157. King, R. B.; Chen, Z.; Schleyer, P. v. R. *Inorg. Chem.* **2004**, *43*, 4564.
(11) Bulusu, S.; Li, X.; Wang, L.-S.; Zeng, X. C. *Proc. Natl. Acad. Sci.* **2006**, *103*, 8326.
(12) Li, J.; Li, X.; Zhai, H.-J.; Wang, L.-S. *Science* **2003**, *299*, 864.
(13) Yoon, B.; Koskinen, P.; Huber, B.; Kostko, O.; von Issendroff, B.; Hakkinen, H.; Moseler, M.; Landman, U. *Chem. Phys. Chem.* **2007**, *8*, 157.
(14) Ercolessi, F.; Andreoni, W.; Tosatti, E. *Phys. Rev. Lett.* **1991**, *66*, 911.
(15) Cleveland, C. L.; Luedtke, W. D.; Landman, U. *Phys. Rev. Lett.* **1998**, *81*, 2036.
(16) Soulé de Bas, B.; Ford, M. J.; Cortie, M. B. *J. Phys. Condens. Matter* **2006**, *18*, 55.
(17) Chacko, S.; Joshi, K.; Kanhere, D. G.; Blundell, S. A. *Phys. Rev. Lett.* **2004**, *92*, 135506.
(18) Joshi, K.; Krishnamurty, S.; Kanhere, D. G. *Phys. Rev. Lett.* **2006**, *96*, 135703.
(19) Aguado, A.; Lopez, J. M. *Phys. Rev. Lett.* **2005**, *94*, 233401.
(20) Joshi, K.; Kanhere, D. G.; Blundell, S. A. *Phys. Rev. B* **2002**, *66*, 155329.
(21) Krishnamurty, S.; Joshi, K.; Kanhere, D. G.; Blundell, S. A. *Phys. Rev. B* **2006**, *73*, 045419.
(22) Chuang, F. C.; Wang, C. Z.; Ogut, S.; Chelikowsky, J. R.; Ho, K. M. *Phys. Rev. B* **2004**, *69*, 165408.
(23) Manninen, K.; Rytkönen, A.; Manninen, M. *Eur. Phys. J.* **2004**, *29*, 39.
(24) Chacko, S.; Kanhere, D. G.; Blundell, S. A. *Phys. Rev. B* **2005**, *71*, 155407.
(25) Lee, M. S.; Chacko, S.; Kanhere, D. G. *J. Chem. Phys.* **2005**, *123*, 164310.
(26) Schmidt, M.; Kusche, R.; Kronmüller, W.; von Issendorf, B.; Haberland, H. *Phys. Rev. Lett.* **1997**, *79*, 99.
(27) Schmidt, M.; Kusche, R.; von Issendorf, B.; Haberland, H. *Nature* (*London*) **1998**, *393*, 238.

(28) Schmidt, M.; Donges, J.; Hippler, T.; Haberland, H. *Phys. Rev. Lett.* **2003**, *90*, 103401.
(29) Haberland, H.; Hippler, T.; Dongres, J.; Kostko, O.; Schmidt, M.; von Issendorf, B. *Phys. Rev. Lett.* **2005**, *94*, 035701.
(30) Shvartsburg, A.; Jarrold, M. F. *Phys. Rev. Lett.* **2000**, *85*, 2530.
(31) Breaux, G. A.; Benirschke, R. C.; Sugai, T.; Kinnear, B. S.; Jarrold, M. F. *Phys. Rev. Lett.* **2003**, *91*, 215508.
(32) Breaux, G. A.; Hillman, D. A.; Neal, C. M.; Benirschke, R. C.; Jarrold, M. F. *J. Am. Chem. Soc.* **2004**, *126*, 8682.
(33) Breaux, G. A.; Neal, C. M.; Cao, B.; Jarrold, M. F. *Phys. Rev. Lett.* **2005**, *94*, 173401.
(34) Breaux, G. A.; Neal, C. M.; Cao, B.; Jarrold, M. F. *Phys. Rev. B* **2005**, *71*, 073410.
(35) Krishnamurty, S.; Chacko, S.; Kanhere, D. G.; Breaux, G. A.; Neal, C. M.; Jarrold, M. F. *Phys. Rev. B* **2006**, *73*, 045406.
(36) Neal, C. M.; Starace, A. K.; Jarrold, M. F.; Joshi, K.; Krishnamurty, S.; Kanhere, D. G. Unpublished results.
(37) Car, R.; Parrinello, M. *Phys. Rev. Lett.* **1985**, *55*, 2471.
(38) Payne, M. C.; Teter, M. P.; Allen, D. C.; Arias, T. A.; Joannopoulos, J. D. *Rev. Mod. Phys.* **1991**, *64*, 1045.
(39) Nose, S. *Mol. Phys.* **1984**, *52*, 255.
(40) We have verified this for a few temperatues in the present work and for several temperatues in other systems such as sodium, tin, silicon, and gallium (unpublished work).
(41) Vanderbilt, D. *Phys. Rev. B* **1990**, *41*, 7892.
(42) *Vienna Ab initio* simulation package, Technische Universität: Wien, 1999. Kresse, G.; Furthmüller, J. *Phys. Rev. B* **1996**, *54*, 11169.
(43) Fernandez, E. M.; Soler, J. M.; Balbas, L. C. *Phys. Rev. B* **2006**, *73*, 235433.
(44) Ferrenberg, A. M.; Swendsen, R. H. *Phys. Rev. Lett.* **1988**, *61*, 2635. Labastie, P.; Whetten, R. L. *Phys. Rev. Lett.* **1990**, *65*, 1567.
(45) Kanhere, D. G.; Vichare, A.; Blundell, S. A. *Reviews in Modern Quantum Chemistry*; Sen, K. D., Ed.; World Scientific: Singapore, 2001.
(46) Chuang, F.-c.; Wang, C. Z.; Ogut, S.; Chelokowsky, J. R.; Ho, K. M. *Phys. Rev. B* **2004**, *69*, 165408.
(47) Bixon, M.; Jortner, J. *J. Chem. Phys.* **1989**, *91*, 1631.
(48) Fratz, D. D. *J. Chem. Phys.* **1995**, *102*, 3747.
(49) The shortest Au−Au bonds in Au_{19} and Au_{20} are distributed along the edges shown Figure 3 in both LDA as well as GGA (PBE exchange correlation functional). The shortest bonds in LDA are 2.64 Å while in the case of GGA they are 2.70 Å. The rest of the first nearest neighbour bond distances are 2.75 and 2.84 Å in LDA and GGA, respectively.